

Mapping the Cosmic Gamma-ray Horizon: The 1CGH Catalogue of Fermi-LAT detections above 10 GeV

Bruno Arsioli,^{1*} Yu-Ling Chang,² Luca Ighina,^{3,4}

¹*Institute of Astrophysics and Space Science, OAL, University of Lisbon, Tapada da Ajuda, 1349-018 Lisbon, Portugal*

²*Graduate Institute of Astrophysics, National Taiwan University, No. 1, Sec. 4, Roosevelt Road, Taipei 10617, Taiwan*

³*Center for Astrophysics | Harvard & Smithsonian, 60 Garden St., Cambridge, MA 02138, USA*

⁴*INAF, Osservatorio Astronomico di Brera, via Brera 28, 20121, Milano, Italy*

28 November 2024

ABSTRACT

We present the First Cosmic Gamma-ray Horizon (1CGH) catalogue, featuring γ -ray detections above 10 GeV based on 16 years of observations with the Fermi-LAT satellite. After carefully selecting a sample of blazars and blazar candidates from catalogues in the literature, we performed a binned likelihood analysis and identified about 2900 γ -ray emitters above 10 GeV, including 69 reported here for the first time. For each source, we estimated the mean energy of the highest-energy bin and analysed them in the context of the cosmic gamma-ray horizon. By adopting a reference model for the Extragalactic Background Light (EBL), we identified a subsample of about 500 sources where moderate to severe γ -ray absorption could be detected across the redshift range of 0 to 3.0. This work provides the most up-to-date compilation of detections above 10 GeV, along with their redshift information. We condense extensive results from the literature, including reports on observational campaigns dedicated to blazars and γ -ray sources, thereby delivering an unprecedented review of the redshift information for sources detected above 10 GeV. Additionally, we highlight key 1CGH sources where redshift information remains incomplete, offering guidance for future optical observation campaigns. The 1CGH catalogue aims to track the most significant sources for understanding the γ -ray transparency of the universe. Furthermore, it provides a targeted subsample where the EBL optical depth, $\tau_{(E,z)}$, can be effectively measured using Fermi-LAT data.

Key words: gamma-rays; galaxies, catalogues – radiation mechanisms: non-thermal

1 INTRODUCTION

Blazars are a rare class of active galactic nuclei (AGN) characterised by relativistic jets pointing towards us, producing non-thermal emission that spans from radio to TeV γ -rays. Ranking among the most luminous and variable sources, blazars provide an unparalleled view into high-energy astrophysical processes, serving as cosmic beacons for studying the transparency of the universe to γ -rays.

The Fermi Large Area Telescope (Fermi-LAT, [Atwood et al. 2009](#)) has revolutionized our understanding of blazars, enabling us to collect data from tens of MeV to hundreds of GeV. Its vast energy coverage allows us to study the interaction of γ -rays with the Extragalactic Background Light (EBL), which leads to attenuation of the very high energy (VHE) spectrum from distant sources. This process is driven by photon-photon annihilation via electron-positron pair production, $\gamma_{\text{VHE}} + \gamma_{\text{EBL}} \rightarrow e^+ + e^-$ ([Nikishov 1961](#); [Gould & Schröder 1967](#)), providing a unique means to use blazars as probes of the EBL density and evolution over cosmic time.

Direct EBL measurements are hindered by the presence of foregrounds, including zodiacal light ([Finke et al. 2022](#)). However, distant extragalactic γ -ray sources, like blazars, provide indirect probes to map the EBL density and distribution throughout cosmic history.

The EBL density in the far ultraviolet (FUV) to near-infrared (NIR) is largely driven by cumulative stellar activity throughout cosmic history ([Hauser & Dwek 2001](#)). Thus, measuring the EBL at a given redshift provides an alternative diagnostic to recover the star formation rate (SFR) from earlier epochs ([Robertson et al. 2010](#)), reaching as far back as the Epoch of Reionization.

Given the sensitivity of Fermi-LAT, observations are particularly well-suited to measuring the EBL in the UV to optical bands, whereas the near-infrared (NIR) can still be constrained at lower redshifts. For example, [Fermi-LAT Collaboration et al. \(2018\)](#) demonstrated how distant γ -ray sources can trace the EBL density to $z \sim 3.0$, providing unique insights into SFR close to the epoch of reionization at $z \sim 6.0$.

The attenuation of γ -rays can be quantified by the EBL optical depth $\tau(E, z)$, which describes the cumulative probability of pair production and provides the relationship between observed and intrinsic flux:

$$F_{\text{observed}} = F_{\text{intrinsic}} \times \exp^{-\tau(E,z)} \quad (1)$$

where a value of $\tau_{(E,z)} = 1$ implies that approximately 63% of the γ -ray flux at energy E from a source at redshift z is absorbed. Measuring $\tau_{(E,z)}$ is essential to understand the transparency of the universe to gamma-rays, and provides a framework for testing and validation of EBL models.

* E-mail: bsarsioli@ciencias.ulisboa.pt & bruno.arsolioli@gmail.com

Interestingly, the very high-energy (VHE) spectra of distant blazars can exhibit an unexpected hardening at the highest energies (Essey & Kusenko 2010; Furniss et al. 2015). This phenomenon has led to alternative hypotheses regarding the propagation of VHE photons, including photon oscillations into axion-like particles (ALPs) (Galanti et al. 2019; Abe et al. 2024) and potential Lorentz invariance violation (LIV) Galanti et al. (2020). These mechanisms offer opportunities to probe fundamental physics and represent open questions in high-energy astrophysics. Therefore, a well-characterised sample of VHE emitters across a broad redshift range is essential –not only to probe EBL and SFR evolution more effectively but also to shed light on alternative photon propagation scenarios.

In this work, we use Fermi-LAT observations spanning 16 years (August 2008 to August 2024) to search for γ -ray signatures associated with a sample of blazars and blazar candidates. By focusing on sources detectable above 10 GeV, we aim to provide a catalogue where the EBL absorption is most pronounced and could be effectively measured in the highest energy bins. To create a robust γ -ray sample suitable for studying EBL attenuation, we calculate the mean energy of the four highest-energy photons detected for each source. This approach offers a more stable and representative measure of the highest energy bin (E_{\max}^{bin}) detectable by Fermi-LAT, particularly when ranking sources that experience moderate to severe absorption, compared to using only the highest-energy photon (E_{\max}).

The First Cosmic Gamma-ray Horizon (ICGH) catalogue represents a significant step forward in describing the γ -ray horizon, and will contribute to our measurements of the EBL content and star formation rate (SFR) across cosmic history. This work builds upon and complements existing efforts, like the 3FHL catalogue (Ajello et al. 2017), and implement several key advancements: a significantly extended observational period, an extensive redshift characterization, and enhanced sensitivity achieved through the use of blazar seed positions during the likelihood analysis. Together, these enhancements enable the identification of weaker sources and provide a more reliable basis for investigating EBL absorption.

In addition, we propose a selection criterion that focus on sources above the $\tau_{(E,z)} > 0.1$ threshold, we build a subsample specifically targeted to the regime where at least 10% of the γ -ray flux is expected to be absorbed in the highest energy bin.

An essential component of this work is the extensive redshift review of the detected sources. Initially, nearly half of them lacked redshift estimates from the reference catalogues (5BZcat, 3HSP, 3FHL, 4LAC-DR3). To address this gap, we conducted a comprehensive literature search, covering nearly 60 publications. We gather information on spectroscopic redshift, lower limit estimates, and uncertain redshift –including photometric estimates. This effort significantly improved the reliability of our redshift data, providing a stronger foundation for subsequent studies.

The ICGH catalogue lays the foundation for advancing our understanding of the transparency of universe to γ -rays. By providing a carefully curated sample of blazars with measurable EBL absorption, our work complements ongoing studies of TeV-detected sources (Gréaux et al. 2023) and aims to deepen the scientific discussion on cosmic γ -ray propagation.

2 DATA ANALYSIS AND METHODS

In this section, we discuss the selection of γ -ray candidates, the data analysis setup using the Fermi Science Tools, and the methods employed for cleaning and associating high-energy photons with sources detected above 10 GeV. We also outline the overall strategy

used to ensure robust detections and photon associations, as reported in the ICGH catalogue.

2.1 Building a Sample of gamma-ray Candidates

To create a sample of sky positions and define our γ -ray targets, we combined several major blazar and AGN catalogues, removing duplicates through internal matching. We began by merging the ‘5th edition of the Roma-BZCAT Multi-Frequency Blazar Catalog’ (5BZcat, Massaro et al. 2015a) with the ‘3rd edition of the High Synchrotron Peak sample’ (3HSP, Chang et al. 2019). These catalogues were chosen for their extensive blazar coverage and reliability.

Both 5BZcat and 3HSP are advanced versions of multifrequency catalogues containing thousands of blazars and blazar candidates. These catalogues have been iteratively refined over time (e.g., refer to BZcat, 1WHSP, and 2WHSP catalogues for earlier versions Massaro et al. 2009; Arsioli et al. 2015; Chang et al. 2017), and represent significant repositories for the very high-energy community.

We also included the latest version (V3.4) of TeVcat (Wakely & Horan 2008), which contains a follow-up list of VHE-detected sources; <http://tevcad.uchicago.edu>. Additionally, to improve the list of seed positions, we incorporate newly confirmed blazars and blazar candidates from recent literature, including Paliya et al. (2020); Maselli et al. (2013); Ighina et al. (2023, 2024).

We further include all sources classified as AGNs, blazars, and blazar candidates in the ‘Fourth Catalog of Active Galactic Nuclei Detected by the Fermi Large Area Telescope: Data Release 3’ (4LAC-DR3, Ajello et al. 2022), since many of those candidates are not covered by the 5BZcat and 3HSP catalogues.

To remove duplicate entries, we use TopCat (Taylor 2005) for internal matching; For the 5BZcat and 3HSP samples, the R.A. and Dec. positions, corresponding to the optical and infrared counterparts respectively, were used. For TeVcat and 4LAC-DR3 sources, we used the associated counterpart position whenever available (e.g., radio, infrared, or optical), as these typically offer better astrometric precision compared to the γ -ray position. With this sample of unique sources, we searched for γ -ray associations in the 4FGL-DR4 catalogue (Ballet et al. 2023) and the 3FHL catalogue (Ajello et al. 2017), considering the 95% containment region reported for each source.

At this point, we have successfully listed unique seed positions recovered from the 5BZcat, 3HSP, TeVcat and 4LAC-DR3 catalogues; But still, many 4FGL-DR4 high-latitude sources ($|b| > 10^\circ$) were not included in our initial sample of 10 GeV candidates. This is partly due to new γ -ray detections from DR4 that had not yet been incorporated into the latest 4LAC release. However, the main reason is that many of these missing sources are actually unassociated in the 4FGL-DR4 –lacking classification.

Therefore, in this work, we consider all unassociated high-latitude 4FGL-DR4 sources as valid 10 GeV candidates. Tracking detections above 10 GeV is essential, as it may motivate observational campaigns for their identification. Furthermore, including unassociated sources in the ICGH catalogue provides an opportunity for serendipitous associations, which could lead to new identifications that enhance our description of the Cosmic Gamma-ray Horizon.

In the final sample of seed positions, we removed all sources flagged as extended and as gamma-ray bursts (GRBs). Finally, we used the *CLASSI* flag from the 4FGL-DR4 catalogue to exclude cases associated with galactic sources (e.g., pwn, lmb, hmb, msp, glc, bin, nov, spp, Ballet et al. 2023). The resulting sample contains approximately 8000 seed positions, with 5023 flagged as blazars or blazar candidates. The remainder are unknown types of sources from 4FGL-DR4 and TeVcat.

Table 1. Power-law model parameters for the top 29 most significant new γ -ray sources discovered in the ICGH catalogue. A complete table with all 2913 ICGH sources is available in the online version of this paper (Note: A preliminary version is available in the Authors' GitHub repository). The first three columns show the original source names, right ascension (R.A.), and declination (Dec.) in degrees (J2000), respectively. The fourth column lists redshifts from literature, marked with a '(?)' flag for uncertain or photometric values, and with a '>' symbol for lower limits. The power-law parameters regarding the ICGH analysis are reported in the following columns, corresponding to the fit (Equation 2): the normalization ' N_0 ' in units of $\text{ph}/\text{cm}^2/\text{s}/\text{MeV}$, the photon spectral index ' Γ ', and the flux integrated over 10-800 GeV, given in units of $\text{ph}/\text{cm}^2/\text{s}$. The pivot energy, ' E_0 ', is fixed at 15 GeV for all sources. The 'TS' column indicates the Test Statistic value. The final column, $E_{\text{max}}^{[\text{GeV}]}$, provides the highest energy photon associated with each ICGH source, based on PASS8 UltraClean event-class, with PSF=0 events removed, i.e. $\text{evclass}=512$ and $\text{evtype}=56$ (see Section 2.3).

Name	R.A. (deg)	Dec. (deg)	z	b(deg)	$N_0 (\times 10^{-16})$	Γ	Flux $^{10-800 \text{ GeV}}$ ($\times 10^{-12}$)	TS	$E_{\text{max}}^{[\text{GeV}]}$
3HSPJ120711.5-174605	181.79787	-17.76830	>0.7	43.83	15.59±4.69	2.90±0.52	26.54±7.82	44.7	37.2
3HSPJ220451.0-181536	331.21379	-18.26011	0.26(?)	-50.75	7.37±3.21	1.91±0.36	17.19±6.28	30.6	51.4
3HSPJ030103.7+344101	45.26558	34.68366	0.246	-21.00	8.95±3.37	2.29±0.51	17.46±5.96	30.5	32.1
3HSPJ132635.9+254958	201.64970	25.83300	0.698	82.02	4.46±2.33	1.62±0.35	12.88±4.97	28.9	116.8
3HSPJ231023.4+311949	347.59737	31.33033	0.48(?)	-26.77	5.30±0.31	1.85±0.11	12.88±1.15	26.1	51.8
3HSPJ155424.1+201125	238.60054	20.19038	0.273	47.76	10.22±4.11	2.09±0.47	21.69±8.78	25.9	138.6
3HSPJ101616.8+410812	154.07008	41.13680	0.27	55.32	4.04±2.22	1.77±0.39	10.39±4.41	24.1	164.2
3HSPJ231041.8-434734	347.67400	-43.79280	0.089	-63.75	3.86±0.30	1.71±0.10	10.37±0.94	23.6	48.7
3HSPJ094606.1+215138	146.52554	21.86066	0.489	47.73	7.27±2.83	2.94±0.77	12.34±4.89	22.0	20.3
3HSPJ091222.9-251825	138.09545	-25.30702	0.33(?)	15.62	7.76±3.04	2.45±0.50	14.41±6.00	21.8	52.1
3HSPJ141003.9+051557	212.51633	5.26605	0.544	61.21	6.99±3.33	2.26±0.51	13.79±5.65	21.6	68.0
3HSPJ061104.1+682956	92.76716	68.49905	0.5(?)	21.53	5.38±0.76	2.29±0.16	10.51±1.57	21.5	58.2
3HSPJ024115.5-304140	40.31454	-30.69447	0.3(?)	-65.76	6.73±1.06	2.25±0.23	13.32±2.33	21.3	59.9
3HSPJ102523.0+040229	156.34595	4.04150	0.208	48.21	6.34±0.38	2.51±0.15	11.57±1.04	20.5	28.7
3HSPJ121038.3-252713	182.65970	-25.45383	0.47(?)	36.50	8.60±1.95	3.22±0.47	14.31±3.25	19.7	26.3
3HSPJ213004.8-563222	322.51987	-56.53947	-	-43.91	5.26±2.47	1.94±0.39	12.06±4.80	18.4	57.2
5BZQJ1353+0151	208.46492	1.86497	1.608	60.64	2.27±0.13	1.41±0.08	8.166±0.73	18.3	55.0
3HSPJ094502.0-044833	146.25845	-4.80938	0.43(?)	34.82	6.95±2.61	2.78±0.65	12.04±4.49	17.8	50.1
3HSPJ120543.3+582933	181.43029	58.49266	0.4(?)	57.63	5.15±2.22	3.44±0.98	8.539±3.68	17.8	24.5
3HSPJ213448.2-164205	323.70091	-16.70155	0.8(?)	-43.51	7.97±3.48	3.63±1.19	13.23±5.74	17.3	29.5
3HSPJ054903.0-215001	87.26416	-21.83369	0.35(?)	-23.05	5.12±2.45	2.46±0.66	9.495±4.17	17.2	66.5
5BZGJ1840-7709	280.16083	-77.15797	0.018	-25.80	5.97±2.57	2.44±0.52	11.10±4.54	16.8	29.8
3HSPJ064326.7+421418	100.86133	42.23852	0.089	16.47	7.31±3.28	2.81±0.72	12.62±5.34	16.5	68.0
3HSPJ100444.8+375212	151.18654	37.87000	0.44	53.58	4.52±0.65	3.86±0.47	7.580±1.11	16.3	13.7
3HSPJ151136.9-165326	227.90375	-16.89077	0.36(?)	34.38	8.68±3.59	3.02±0.82	14.63±5.93	16.3	30.8
3HSPJ104745.8+543741	161.94087	54.62813	0.54(?)	54.46	4.56±2.07	2.61±0.71	8.165±3.64	16.3	31.7
3HSPJ081941.8+053023	124.92433	5.50638	0.37(?)	22.11	7.02±3.26	2.80±0.75	12.14±5.52	16.2	17.0
3HSPJ062753.4-151957	96.97237	-15.33252	0.29(?)	-12.04	5.32±2.89	1.85±0.41	12.89±5.63	16.2	38.8
3HSPJ133326.0+623541	203.35820	62.59494	0.48(?)	53.86	1.69±0.10	1.43±0.08	5.954±0.35	16.0	93.2

2.2 Broadband Likelihood Analysis with Fermi Science Tools

To search for γ -ray signatures associated with the pre-selected seed positions, we performed a binned likelihood analysis in the 10-800 GeV band, covering 16 years of Fermi-LAT observations (August 2008 to August 2024). The analysis used the latest version of the *Fermi Science Tools* (V2.2.0)¹, with Pass 8 event selection (P8R3, Atwood et al. 2013; Bruel et al. 2018).

For the broadband analysis, we followed the recommendations from the Fermi-LAT team to identify point-like sources. We used FRONT+BACK source-class events ($\text{evtype}=3$ and $\text{evclass}=128$)

and the instrument response function (IRF) P8R3-SOURCE-V3. For each analysis, we considered a region of interest (ROI) of 15° radius centred on the γ -ray seed positions. For modelling the background of point and extended sources, we adopted the 4FGL-DR4 v34 catalogue (*gll-psc-v34.fit*), along with isotropic and galactic-diffuse templates (*iso-P8R3-SOURCE-V3-v1.txt* and *gll-iem-uw1216-v13.fits*, respectively). The spectral parameters –normalization and photon index– were set free for all sources within 5° of the seed position.

A zenith angle cut of 105° was applied to avoid contamination from Earth's limb γ -ray photons, which are produced by cosmic-ray interactions with the atmosphere. Using the `gtmktime` routine, we select good time intervals when Fermi-LAT was operating in 'science data-taking mode,' by setting the flags `DATA-QUAL>0` and `LAT-CONFIG==1`. Using the `gtbin` routine, we generated counts maps (CMAP) and counts cubes (CCUBE) with dimensions of $300 \times$

¹ The FermiTools-Conda repository: <https://github.com/fermi-lat/FermiTools-Conda>. The Fermi-LAT data analysis recommendations: <https://fermi.gsfc.nasa.gov/ssc/data/analysis/>.

300 and 200×200 pixels at $0.1^\circ/\text{pixel}$, respectively. For the CCUBE, we used 20 equally-spaced logarithmic energy bins in the 10–800 GeV range. Each candidate was modelled as a point-like source within the region of interest (ROI) and characterised by a power-law spectrum:

$$\frac{dN}{dE} = N_0 \left(\frac{E}{E_0} \right)^{-\Gamma}, \quad (2)$$

In this equation, N_0 is the normalization constant (prefactor), given in units of [photons/cm²/s/MeV], representing the flux density at the pivot energy E_0 . The parameter Γ represents the photon spectral index, indicating the slope of the spectrum.

The use of multifrequency seed positions for detecting γ -ray sources has been successfully applied in numerous works (Arsioli & Chang 2017; Arsioli et al. 2018; Arsioli & Polenta 2018; Arsioli et al. 2020). This approach has proven effective in unveiling extreme blazars close to the Fermi-LAT detection threshold, providing a reliable starting point for in-depth γ -ray analyses. Using this approach, the analysis for each sky position is therefore independent –probing a single γ -ray candidate at a time. To handle all 8000 candidates efficiently, we relied on parallel High Performance Computing (HPC) resources provided by INCD-Portugal.

Blazars are known to be the dominant extragalactic population of GeV emitters. Considering our likelihood analysis involves only two degrees of freedom (Γ and N_0) we adopted a pre-selection threshold² of $TS > 10$ to include faint sources for potential future follow-up observations. As suggested in Mattox et al. (1996) –and latter implemented in Arsioli et al. (2020)– the use of multifrequency seeds improves γ -ray detection of point-like sources near the Fermi-LAT threshold, making it a robust strategy for data exploration.

In the next section, we discuss additional selection criteria adopted to avoid spurious detections while building the ICGH catalogue.

2.3 Fermi-LAT Events Sample Above 10 GeV

As a result of the likelihood analysis, we pre-selected approximately 3200 sources with $TS > 10$. To investigate the cosmic gamma-ray horizon, we need to examine the Fermi-LAT data to identify the highest-energy events associated with each pre-selected source. It is essential to consider the different event types in the Fermi-LAT dataset and also to identify and remove potential sources of contamination from the events sample.

In the Fermi-LAT PASS8 release (Atwood et al. 2013), each event is assigned a Point Spread Function (PSF) type, which indicates the quality of the reconstructed direction. Events are categorized into four quartiles: PSF0 (lowest-quality, $evtype=4$), PSF1 ($evtype=8$), PSF2 ($evtype=16$), and PSF3 (highest-quality, $evtype=32$). The PSF 68% containment radius varies by energy and event type. For instance, at 30 GeV, the containment radius for PSF1 events is approximately 0.12° , as described in PASS8 documentation³.

Using the `gtselect` routine, we created a subsample of the all-sky Fermi-LAT data, selecting only events with energy greater than 10 GeV. We removed low-quality events by excluding PSF0 events, which represent the quartile with the poorest reconstruction accuracy.

² The Test Statistic (TS) parameter is defined as $-2 \ln(L_{(\text{no-source})} \div L_{(\text{source})})$, where $L_{(\text{no-source})}$ represents the likelihood of observing a given photon count due to background alone (the null hypothesis), and $L_{(\text{source})}$ represents the likelihood of observing the photon count assuming a source exists at a particular position (Mattox et al. 1996).

³ Fermi-LAT PASS8 PSF: https://www.slac.stanford.edu/exp/glast/groups/canda/lat_Performance.htm

Next, we used the `gtmktime` routine to select events during good time intervals (see Section 2.2). After this step, we were left with a photon sample containing PSF1–2–3 source-type events (i.e., $evclass=128$ and $evtype=56$), with a maximum zenith angle of 105° , all recorded under ‘science data-taking mode’.

Before recovering the γ -ray events associated with the pre-selected sources, we applied an additional layer of data cleaning to improve the quality of the photon sample. Specifically, we removed events associated with solar emissions and gamma-ray bursts (GRBs). Indeed the solar disk has recently been confirmed as a source of very high-energy γ -rays (Linden et al. 2022; Albert et al. 2023; Arsioli & Orlando 2024); Therefore, we removed all events that might be linked to solar emissions by assuming an association radius of 0.8° ⁴.

To identify and remove events related to GRBs, we used the Fermi GBM Burst Catalogue⁵ (von Kienlin et al. 2020). We removed events recorded within 0.8° of GRB locations, also considering a time window of 30 minutes before and 10 hours after each GRB.

The characteristic position uncertainty of PSF1 events at 30 GeV was used as a basis for defining a cross-matching radius of 0.12° between the pre-selected candidates and the clean photon sample. This conservative radius ensures robustness when associating higher-energy events, particularly given the larger PSF1 size at the lowest energy (approximately 0.18° at 10 GeV).

For the final selection layer of the ICGH catalogue, we retained only pre-selected sources ($TS > 10$) that were associated with at least four high-energy events from the clean photon sample, matching within 0.12° . This approach follows similar criteria used in building the 3FHL sample (Ajello et al. 2017), which required a minimum of four associated photons for source acceptance (as predicted by the adjusted model, i.e., $N_{pred} \geq 4$).

3 THE FIRST COSMIC GAMMA-RAY HORIZON CATALOGUE: ICGH

We present the First Cosmic Gamma-ray Horizon catalogue (ICGH), which lists 2913 blazars and blazar candidates detected with a TS greater than 10 in the 10–800 GeV energy range, integrated over 16 years of Fermi-LAT observations.

The ICGH catalogue includes 69 γ -ray detections never reported in earlier Fermi-LAT catalogue releases (1FGL, 2FGL, 3FGL, or 4FGL), representing entirely new γ -ray sources. These newly identified sources could be especially significant as candidates for very high-energy (VHE) observations with the upcoming Cherenkov Telescope Array Observatory (CTAO) (CTAO, Cherenkov Telescope Array Consortium et al. 2019; Acharya et al. 2013).

Table 1 presents a selection of newly detected sources with TS above 16, including the seed-source name, right ascension (R.A.), declination (Dec.), redshift, and power-law model parameters associated with each new γ -ray detection⁶.

⁴ Considering the solar disk has an angular radius of approximately 0.26° , and the characteristic scale of position uncertainty for PSF1 events at 10 GeV is around 0.18° , a 0.8° radius cut safely encompasses and removes solar disk contamination.

⁵ The continuously updated GBM Burst Catalogue, also referred to as ‘The FERMIGBRST database’, is available at <https://heasarc.gsfc.nasa.gov/W3Browse/fermi/fermigbrst.html>.

⁶ The First Cosmic Gamma-ray Horizon catalogue will be available in public data repositories such as Vizier <https://vizier.cds.unistra.fr/viz-bin/VizieR> and GitHub <https://github.com/BrunoArsioli>.

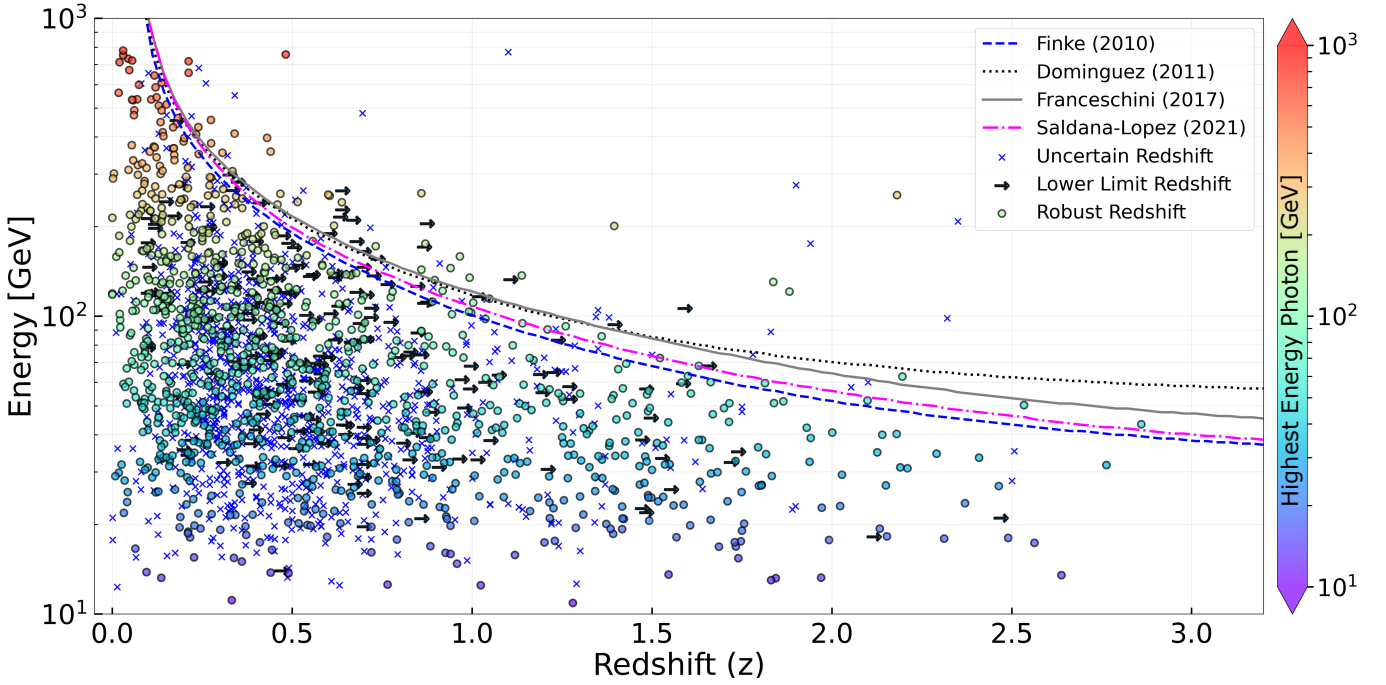


Figure 1. The cosmic gamma-ray horizon, showing the highest-energy photon versus redshift, based on Fermi-LAT ultra-clean events with PSF0 events removed (`evclass=512` and `evtype=56`). Sources detected above 10 GeV are represented, with robust (spectroscopic) redshifts marked as filled circles, lower limit redshifts shown as right arrows, and uncertain redshifts (photometric or reported as doubtful) indicated by blue crosses. The EBL optical depth $\tau_{(E,z)} = 1.0$ is depicted for different models: [Finke et al. \(2010\)](#) (blue dashed line), [Domínguez et al. \(2011\)](#) (black dotted line), [Franceschini & Rodighiero \(2017\)](#) (grey line), and [Saldana-Lopez et al. \(2021\)](#) (magenta dot-dashed line). For better visualization, the photon energy of sources with robust redshift is colour-coded. Note that approximately one-third of the ICGH sources lack assigned redshift and are therefore not included in this plot.

3.1 Our Major Redshift Review

In addition to listing detections above 10 GeV, we conducted an extensive literature review to improve the redshift characterization of our sample, which is crucial for investigating the cosmic γ -ray horizon. Based on the latest studies, we revised and updated redshift information, tracked the origin and quality of the data, and incorporated new redshifts from multiple optical campaigns dedicated to characterizing blazars, 3FHL and 4FGL sources. To track redshift quality, we added a column named ‘z-flag’ to the catalogue, with values: (1) for robust spectroscopic redshift; (2) for photometric estimates or uncertain values (as reported in the literature); and (3) for lower-limit redshift values.

In the ICGH catalogue, we added a column named ‘z-origin’ to track the origin of the redshift values reported in the ‘z’ column. Redshift information was gathered from several major blazar and γ -ray catalogues, including 5BZcat ([Massaro et al. 2015a](#)), 3HSPcat ([Chang et al. 2019](#)), 4LACdre ([Ajello et al. 2022](#)), and TeVcat ([Wakely & Horan 2008](#)). Additionally, redshift values were extracted from dedicated observational campaigns, such as Boyle90 ([Boyle et al. 1990](#)), Maisner10 ([Meisner & Romani 2010](#)); Pulido10 ([Acosta-Pulido et al. 2010](#)); Shaw12 ([Shaw et al. 2012](#)); Furniss13 ([Furniss et al. 2013](#)); Maselli13 ([Maselli et al. 2013](#)); Rovero13 ([Rovero et al. 2013](#)); Sadrinelli13 ([Sandrinelli et al. 2013](#)); Shaw13 ([Shaw et al. 2013](#)); Paggi14 ([Paggi et al. 2014](#)); Ricci15 ([Ricci et al. 2015](#)); AlvarezCrespo16a-b-c ([Álvarez Crespo et al. 2016a,b,c](#)); Kaur16 ([Kaur et al. 2017](#)); Rovero16 ([Rovero et al. 2015, 2016](#)); Juanita17 ([Torres-Zafra et al. 2018](#)); Paiano17 ([Paiano et al. 2017b,a](#)); Gabanyi18 ([Gábányi et al. 2018](#)); Landoni18 ([Landoni et al. 2015, 2018](#)); Massaro18 ([Massaro et al. 2014, 2015b, 2016](#)); Balmaverde19

([Balmaverde et al. 2020](#)); Caccianiga19 ([Caccianiga et al. 2019](#)); Johnson19 ([Johnson et al. 2019](#)); Desai19 ([Desai et al. 2019](#)); Menezes19 ([de Menezes et al. 2019, 2020](#)); Marchesini19 ([Marchesini et al. 2019](#)); Belladitta20 ([Belladitta et al. 2020](#)); Goldoni20 ([Goldoni et al. 2015, 2021](#)); Pena-Herazo20 ([Peña-Herazo et al. 2020, 2019, 2017](#)); Paiano20 ([Paiano et al. 2019, 2020](#)); Raiteri20 ([Raiteri et al. 2020](#)); Pena-Herazo21 ([Peña-Herazo et al. 2021b,a](#)); B.Gonzalez21 ([Becerra González et al. 2021](#)); Rajagopal21 ([Rajagopal et al. 2021](#)); Foschini22 ([Foschini et al. 2022](#)); Kasai22 ([Kasai et al. 2023b,a](#)); OlmoGarcia22 ([Olmo-García et al. 2022](#)); Rajagopal22 ([Rajagopal et al. 2023](#)); Ammando24 ([D’Ammando et al. 2012, 2024](#)); and Sarira24 ([Sahu et al. 2024](#)).

This represents a substantial improvement over existing catalogues, such as 4LAC-DR3, which do not differentiate between spectroscopic and photometric redshift⁷. In fact, the numerous dedicated optical observation campaigns highlight the ongoing high demand for the characterization of blazars and blazar candidates, particularly in connection with their γ -ray counterparts.

Extensive redshift characterization is key for samples used to study the cosmic gamma-ray horizon, as it helps to mitigate biases caused by missing or uncertain redshift values. The best way to reduce uncertainties when measuring the EBL density evolution is to increase the number of sources with robust redshift determinations. In particular, identifying absorbed sources above redshift 2.0 would significantly improve EBL measurement at a regime that impacts SFR density estimates near and within the EoR, at $z \sim 6-7$ Fermi-LAT

⁷ Please, refer to sec. 5.2 from [Ajello et al. \(2020\)](#) about the 4LAC redshift contamination with photometric values.

Collaboration et al. (2018). With increased precision in EBL density measurements, we can potentially disentangle the contributions of star formation and active galactic nuclei (AGN) to the EBL buildup at high redshift, providing a complementary probe for assessing the AGN contribution during the EoR.

3.2 The Cosmic Gamma-ray Horizon Plot

Plotting the highest-energy photons from the ICGH catalogue against redshift reveals that the universe is indeed opaque to γ -rays, as predicted by Nikishov (1961); Gould & Schröder (1967). The energy vs. redshift relationship, where the opacity $\tau(E, z) = 1.0$, defines what is known as the ‘Cosmic Gamma-Ray Horizon’. Beyond this horizon, high-energy photons are severely attenuated by the EBL, rendering the universe effectively opaque to γ -rays.

Figure 1 shows the highest-energy photon versus redshift for the ICGH sources, along with the predicted gamma-ray horizon according to the main EBL models (Finke et al. 2010; Domínguez et al. 2011; Franceschini & Rodighiero 2017; Saldana-Lopez et al. 2021). Different markers are used to represent robust (spectroscopic), photometric/uncertain, and lower limit redshift values to emphasize the importance of accurate redshift determination.

Figure 1 provides an unprecedented view on the redshift characterization of sources used to study the cosmic γ -ray horizon. It highlights the significance of extensive redshift information and aims to further motivate the community’s ongoing efforts in the optical characterization of these rare sources (see Section 3.1). By presenting this detailed view, we emphasize the critical role that redshift characterization plays in advancing our understanding of the γ -ray transparency and EBL models.

3.3 Flagging Source Under Moderate to Severe Absorption

To measure the EBL optical depth, one needs to build the γ -ray spectrum and compare the observed flux with the expected flux as a function of energy. For sources observed with Fermi-LAT, the γ -ray spectrum typically spans from tens of MeV to hundreds of GeV, with flux estimates available for a dozen of energy bins (E^{bin}).

If we look for the most interesting sources for studying the cosmic gamma-ray horizon, we should focus on estimating the largest energy bin ($E_{\text{max}}^{\text{bin}}$) where a source can still be detected. Any source with at least one energy bin experiencing a detectable degree of EBL attenuation is relevant for measuring $\tau_{(E,z)}$ values.

To emphasize sources that could be used to measure $\tau_{(E,z)}$, we developed a selection method based on the $(z, E_{\text{max}}^{\text{bin}})$ position in the energy versus redshift plane. We calculate $E_{\text{max}}^{\text{bin}}$ as the mean energy of the four highest-energy photons associated with a source, to create a robust estimate of the highest energy bin. This approach requires at least four photons to ensure robustness for E^{bin} detection at energies above 10 GeV. A similar requirement for minimum photon counts was applied in the 3FHL catalogue (Ajello et al. 2017) to set a lower acceptance level for robust source detections. For calculating $E_{\text{max}}^{\text{bin}}$, we use the clean photon sample (as described in Section 2.3), considering source-type events and excluding PSF0 events (i.e., `evclass=128` and `evtype=56`).

In Figure 2, we illustrate the energy versus redshift relation and use the Saldana-Lopez EBL model Saldana-Lopez et al. (2021) as a reference framework to identify sources where gamma-ray absorption might be detectable. Our ultimate goal, however, is to highlight a sample in which $\tau_{(E,z)}$ values can be derived from the data, independent of any specific EBL model. The predictions of Saldana-Lopez

are similar to those by Finke et al. (2010) and represent the most severe attenuation among the models considered in this work.

We use an EBL optical depth of $\tau_{(E,z)} = 0.1$ as a lower limit to introduce an absorption flag (ABS-flag), indicating whether spectral absorption might be detectable at the highest energy bins. For cases where $E_{\text{max}}^{\text{bin}}$ lies in the $\tau_{(E,z)} > 0.1$ regime, the largest energy bin observed with Fermi-LAT likely experiences a detectable absorption greater than 10% (i.e., $>(1 - e^{-0.1})$). These sources can be used to measure opacity along redshift, and have an ABS-flag set to ‘1’.

For sources with $E_{\text{max}}^{\text{bin}}$ in the $\tau_{(E,z)} < 0.1$ regime, the Fermi-LAT spectrum is likely unaffected by EBL attenuation, and these sources have an ABS-flag set to ‘0’ in the ICGH catalogue. These sources can be used to study the intrinsic γ -ray spectrum from blazars, helping to refine assumptions regarding their intrinsic flux.

The $\tau_{(E,z)}$ values –calculated using the Saldana-Lopez EBL model at $E_{\text{max}}^{\text{bin}}$ Saldana-Lopez et al. (2021)– are listed under the column ‘ τ_{Ebin} ’. Additionally, the absorption fraction $(1 - e^{-\tau_{(E,z)}})$ is recorded in the ‘Abs_{Ebin}’ column, which can be used to create subsamples based on different absorption thresholds. Notably, for sources with multiple energy bins experiencing detectable absorption, a single source can provide $\tau_{(E,z)}$ estimates for multiple energy levels at a given redshift.

3.4 Best Candidates for Optical Observation Campaigns

Following an extensive review of redshift information, Appendix A highlights the high galactic latitude sources ($|b| > 10^\circ$) that are currently the best candidates for optical observations. We have identified two main types of sources to prioritize, which will further improve the catalogue and the science described above:

- ICGH sources that currently lack redshift information (z -flag = 0) but already have an optical or radio association are prioritised based on $E_{\text{max}}^{\text{bin}}$, the highest energy bin detected with Fermi-LAT. These sources are particularly significant due to the presence of a clear counterpart for optical follow-up and their potential proximity to the $\tau \sim 1.0$ horizon. Table A highlights 44 of these cases.
- ICGH sources with lower limit redshifts or photometric/uncertain redshifts (z -flag = 2 or 3) are prioritised based on their calculated opacity (τ_{Ebin}), using $E_{\text{max}}^{\text{bin}}$ values. These sources could be experiencing significant γ -ray absorption, potentially detectable across multiple energy bins, and thus could provide valuable $\tau_{(E)}$ measurements across different energies at a given redshift. Table A highlight 44 of these cases.

4 SUMMARY AND CONCLUSIONS

In this work, we presented the First Cosmic Gamma-ray Horizon (ICGH) catalogue, which lists all-sky Fermi-LAT detections above 10 GeV, compiled from 16 years of observations. The catalogue includes 2913 sources, with 69 representing new gamma-ray detections and, to date, it represents the most suited sample to study the transparency of the universe to gamma rays.

We significantly improved the redshift characterization of our sample by revising literature and incorporating spectroscopic redshift estimates whenever possible. By meticulously reviewing nearly 60 dedicated observational campaigns, we reduced a substantial portion of the redshift knowledge-gap, categorising redshift reliability through our z -flag system. This improved redshift description provides a solid foundation to investigate EBL-induced attenuation of VHE sources, offering a basis for cosmic gamma-ray horizon studies.

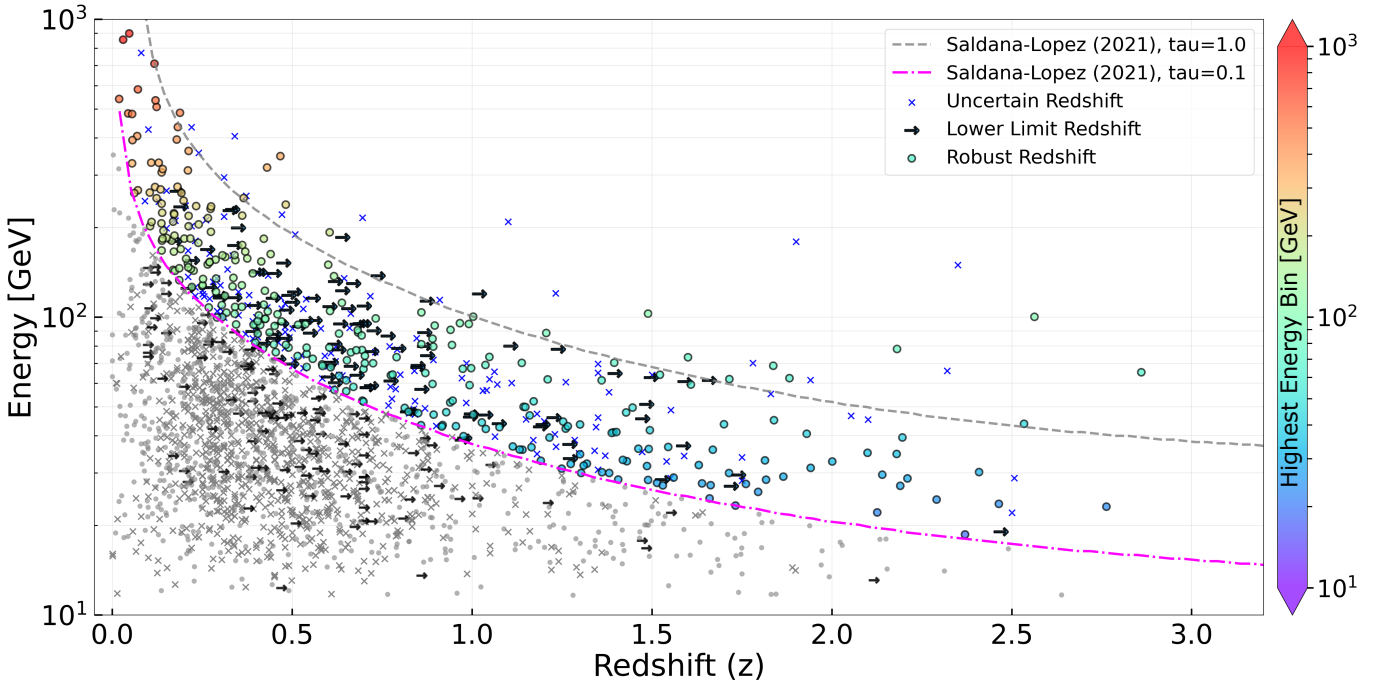


Figure 2. The cosmic gamma-ray horizon, showing the ‘largest energy bin detectable with Fermi-LAT’ versus redshift. The ‘largest energy bin’ is calculated as the mean energy of the four highest-energy source-type events associated with each source, excluding PSF0 events (i.e., `evclass=128` and `evtype=56`). The opacity regimes for EBL optical depths $\tau_{(E,z)} = 1.0$ and $\tau_{(E,z)} = 0.1$ are represented by grey dashed and magenta dot-dashed lines, respectively, corresponding to the Saldana-Lopez model (Saldana-Lopez et al. 2021). This plot highlights sources in the $\tau_{(E,z)} > 0.1$ regime where absorption may be detectable at the highest energy bin observed with Fermi-LAT, while sources in the $\tau < 0.1$ regime are represented by grey markers. Different markers indicate the quality of the redshift determination: robust (spectroscopic) redshifts are shown as filled circles, lower limit redshifts are indicated by right arrows, and uncertain redshifts (photometric or unknown quality) are represented by blue crosses. Approximately one-third of the ICGH sources lack redshift assignments and are therefore not included in this plot.

The ICGH catalogue highlights sources experiencing varying degrees of gamma-ray attenuation, contributing to a better determination of the EBL’s density and its evolution over cosmic time. Using the Saldana-Lopez EBL model as a reference framework, we identified sources with gamma-ray absorption above the $\tau_{(E,z)} > 0.1$ limit, creating a targeted sample where absorption is likely measurable.

In addition, we introduced a complementary data-exploration method by calculating the mean energy of the four highest-energy photons E_{\max}^{bin} , rather than focusing solely on the highest-energy event. This provides a more stable and statistically reliable measure of the characteristic ‘largest energy level’ observed for each source.

We have identified sources that should be prioritised for follow-up optical observation campaigns. These include: (i) sources that lack redshift information but have a clear optical or radio association, prioritised based on the highest E_{\max}^{bin} values; and (ii) sources with lower limit or uncertain redshift estimates that could benefit from further spectroscopic exploration, prioritised by their current τ values at E_{\max}^{bin} . These targets will not only help refine the redshift description of the catalogue but also improve the accuracy of EBL measurements at higher redshifts, thereby reducing uncertainties in SFR density determination during the Epoch of Reionization ($z \sim 6-7$).

ACKNOWLEDGEMENTS

BA thanks the Institute of Astrophysics and Space Sciences (IA) at the University of Lisbon for their ongoing support. BA is currently a Marie Skłodowska-Curie Postdoctoral Fellow at IA, funded by

the European Union’s Horizon 2020 research and innovation program under the MSCA agreement No. 101066981. BA also acknowledges the support from ‘Fundação para a Ciência e a Tecnologia’ (FCT) through the research grant UIDP/04434/2020 (DOI: 10.54499/UIDP/04434/2020) in support of general IA activities. This work was produced with the support of the “National Distributed Computing Infrastructure” (INCD), Portugal (<https://www.incd.pt/>), funded by FCT and FEDER under project 01/SAICT/2016 No. 022153. We acknowledge FCT’s support through the A1 Computation Call (project: 2023.09549.CPCA.A1) for the allocation of HPC resources at INCD. We are grateful to the entire *Fermi*-LAT collaboration for maintaining a publicly accessible mission database, enabling discoveries across the entire γ -ray community. We also utilised archival data and bibliographic information from the NASA-IPAC Extragalactic Database (NED), and data/software facilities maintained by the Space Science Data Center (SSDC) from the Italian Space Agency. We extend our thanks to the TeVcat team, especially Deirdre Horan and Scott Wakely, for their continuous work on VHE detections, as well as NASA and NSF for their support of these follow-up efforts.

DATA AVAILABILITY

All catalogues used to build the sample of γ -ray candidates are publicly available and cited within this work. The ICGH catalogue will be made publicly available through VizieR at <https://vizier.cds.unistra.fr/>, and GitHub. The Fermi-LAT database and the

Science Tools used to build the ICGH catalogue are also publicly accessible at <https://fermi.gsfc.nasa.gov/ssc/data/access/>.

REFERENCES

- Abe H., et al., 2024, *Physics of the Dark Universe*, **44**, 101425
- Acharya B. S., et al., 2013, *Astroparticle Physics*, **43**, 3
- Acosta-Pulido J. A., Agudo I., Barrena R., Ramos Almeida C., Manchado A., Rodríguez-Gil P., 2010, *A&A*, **519**, A5
- Ajello M., et al., 2017, *ApJS*, **232**, 18
- Ajello M., et al., 2020, *ApJ*, **892**, 105
- Ajello M., et al., 2022, *ApJS*, **263**, 24
- Albert A., et al., 2023, *Phys. Rev. Lett.*, **131**, 051201
- Álvarez Crespo N., et al., 2016a, *AJ*, **151**, 32
- Álvarez Crespo N., et al., 2016b, *AJ*, **151**, 95
- Álvarez Crespo N., et al., 2016c, *Ap&SS*, **361**, 316
- Arsioli B., Chang Y. L., 2017, *A&A*, **598**, A134
- Arsioli B., Orlando E., 2024, *ApJ*, **962**, 52
- Arsioli B., Polenta G., 2018, *A&A*, **616**, A20
- Arsioli B., Fraga B., Giommi P., Padovani P., Marrese P. M., 2015, *A&A*, **579**, A34
- Arsioli B., Barres de Almeida U., Prandini E., Fraga B., Foffano L., 2018, *MNRAS*, **480**, 2165
- Arsioli B., Chang Y. L., Musiimenta B., 2020, *MNRAS*, **493**, 2438
- Atwood W. B., et al., 2009, *ApJ*, **697**, 1071
- Atwood W., et al., 2013, *arXiv e-prints*, p. [arXiv:1303.3514](https://arxiv.org/abs/1303.3514)
- Ballet J., Bruel P., Burnett T. H., Lott B., The Fermi-LAT collaboration 2023, *arXiv e-prints*, p. [arXiv:2307.12546](https://arxiv.org/abs/2307.12546)
- Balmaverde B., et al., 2020, *MNRAS*, **492**, 3728
- Becerra González J., Acosta-Pulido J. A., Boschín W., Clavero R., Otero-Santos J., Carballo-Bello J. A., Domínguez-Palmero L., 2021, *MNRAS*, **504**, 5258
- Belladitta S., et al., 2020, *A&A*, **635**, L7
- Boyle B. J., Fong R., Shanks T., Peterson B. A., 1990, *MNRAS*, **243**, 1
- Bruel P., Burnett T. H., Digel S. W., Johannesson G., Omodei N., Wood M., 2018, *arXiv e-prints*, p. [arXiv:1810.11394](https://arxiv.org/abs/1810.11394)
- Caccianiga A., et al., 2019, *MNRAS*, **484**, 204
- Chang Y. L., Arsioli B., Giommi P., Padovani P., 2017, *A&A*, **598**, A17
- Chang Y. L., Arsioli B., Giommi P., Padovani P., Brandt C. H., 2019, *A&A*, **632**, A77
- Cherenkov Telescope Array Consortium et al., 2019, *Science with the Cherenkov Telescope Array*. World Scientific Publishing, doi:10.1142/10986
- D’Ammando F., et al., 2012, *MNRAS*, **427**, 893
- D’Ammando F., et al., 2024, *A&A*, **683**, A222
- Desai A., Marchesi S., Rajagopal M., Ajello M., 2019, *ApJS*, **241**, 5
- Domínguez A., et al., 2011, *MNRAS*, **410**, 2556
- Essey W., Kusenko A., 2010, *Astroparticle Physics*, **33**, 81
- Fermi-LAT Collaboration et al., 2018, *Science*, **362**, 1031
- Finke J. D., Razzaque S., Dermer C. D., 2010, *ApJ*, **712**, 238
- Finke J. D., Ajello M., Domínguez A., Desai A., Hartmann D. H., Paliya V. S., Saldana-Lopez A., 2022, *ApJ*, **941**, 33
- Foschini L., et al., 2022, *Universe*, **8**, 587
- Franceschini A., Rodighiero G., 2017, *A&A*, **603**, A34
- Furniss A., Fumagalli M., Danforth C., Williams D. A., Prochaska J. X., 2013, *ApJ*, **766**, 35
- Furniss A., Sutter P. M., Primack J. R., Domínguez A., 2015, *MNRAS*, **446**, 2267
- Gabányi K. É., Frey S., An T., 2018, *A&A*, **612**, A109
- Galanti G., Tavecchio F., Roncadelli M., Evoli C., 2019, *MNRAS*, **487**, 123
- Galanti G., Tavecchio F., Landoni M., 2020, *MNRAS*, **491**, 5268
- Goldoni P., Pita S., Boisson C., Cotter G., Williams D., Lindfors E., 2015, in 34th International Cosmic Ray Conference (ICRC2015). p. 835 ([arXiv:1508.06059](https://arxiv.org/abs/1508.06059)), doi:10.22323/1.236.0835
- Goldoni P., et al., 2021, *A&A*, **650**, A106
- Gould R. J., Schröder G. P., 1967, *Physical Review*, **155**, 1408
- Gréaux L., Biteau J., Hassan T., Hervet O., Nieves Rosillo M., Williams D. A., 2023, *arXiv e-prints*, p. [arXiv:2304.00835](https://arxiv.org/abs/2304.00835)
- Hauser M. G., Dwek E., 2001, *ARA&A*, **39**, 249
- Ighina L., Caccianiga A., Moretti A., Belladitta S., Broderick J. W., Drouart G., Leung J. K., Seymour N., 2023, *MNRAS*, **519**, 2060
- Ighina L., et al., 2024, *arXiv e-prints*, p. [arXiv:2407.04094](https://arxiv.org/abs/2407.04094)
- Johnson S. D., et al., 2019, *ApJ*, **884**, L31
- Kasai E., Goldoni P., Pita S., Boisson C., Backes M., Cotter G., D’Ammando F., van Soelen B., 2023a, in Liodakis I., Aller M. F., Krawczynski H., Lähteenmäki A., Pearson T. J., eds, IAU Symposium Vol. 375, The Multimessenger Chakra of Blazar Jets. pp 96–100 ([arXiv:2303.12871](https://arxiv.org/abs/2303.12871)), doi:10.1017/S1743921323000789
- Kasai E., et al., 2023b, *MNRAS*, **518**, 2675
- Kaur A., et al., 2017, *ApJ*, **834**, 41
- Landoni M., et al., 2015, *AJ*, **149**, 163
- Landoni M., Paiano S., Falomo R., Scarpa R., Treves A., 2018, *ApJ*, **861**, 130
- Linden T., Beacom J. F., Peter A. H. G., Buckman B. J., Zhou B., Zhu G., 2022, *Phys. Rev. D*, **105**, 063013
- Marchesini E. J., et al., 2019, *Ap&SS*, **364**, 5
- Maselli A., et al., 2013, *ApJS*, **206**, 17
- Massaro E., Giommi P., Leto C., Marchegiani P., Maselli A., Perri M., Piranomonte S., Sclavi S., 2009, *A&A*, **495**, 691
- Massaro F., Masetti N., D’Abrusco R., Paggi A., Funk S., 2014, *AJ*, **148**, 66
- Massaro E., Maselli A., Leto C., Marchegiani P., Perri M., Giommi P., Piranomonte S., 2015a, *Ap&SS*, **357**, 75
- Massaro F., Landoni M., D’Abrusco R., Milisavljevic D., Paggi A., Masetti N., Smith H. A., Tosti G., 2015b, *A&A*, **575**, A124
- Massaro F., et al., 2016, *Ap&SS*, **361**, 337
- Mattox J. R., et al., 1996, *ApJ*, **461**, 396
- Meisner A. M., Romani R. W., 2010, *ApJ*, **712**, 14
- Nikishov A. I., 1961, *Zhur. Ekspit’ i Teoret. Fiz.*, **41**
- Olmo-García A., Paliya V. S., Álvarez Crespo N., Kumar B., Domínguez A., Gil de Paz A., Sánchez-Blázquez P., 2022, *MNRAS*, **516**, 5702
- Paggi A., et al., 2014, *AJ*, **147**, 112
- Paiano S., Landoni M., Falomo R., Treves A., Scarpa R., Righi C., 2017a, *ApJ*, **837**, 144
- Paiano S., Falomo R., Franceschini A., Treves A., Scarpa R., 2017b, *ApJ*, **851**, 135
- Paiano S., Falomo R., Treves A., Franceschini A., Scarpa R., 2019, *ApJ*, **871**, 162
- Paiano S., Falomo R., Treves A., Scarpa R., 2020, *MNRAS*, **497**, 94
- Paliya V. S., Ajello M., Cao H. M., Giroletti M., Kaur A., Madejski G., Lott B., Hartmann D., 2020, *ApJ*, **897**, 177
- Peña-Herazo H. A., et al., 2017, *Ap&SS*, **362**, 228
- Peña-Herazo H. A., et al., 2019, *Ap&SS*, **364**, 85
- Peña-Herazo H. A., et al., 2020, *A&A*, **643**, A103
- Peña-Herazo H. A., et al., 2021a, *AJ*, **161**, 196
- Peña-Herazo H. A., et al., 2021b, *AJ*, **162**, 177
- Raiteri C. M., Acosta Pulido J. A., Villata M., Carnerero M. I., Romano P., Vercellone S., 2020, *MNRAS*, **493**, 2793
- Rajagopal M., Marchesi S., Kaur A., Domínguez A., Silver R., Ajello M., 2021, *ApJS*, **254**, 26
- Rajagopal M., Marcotulli L., Labrie K., Marchesi S., Ajello M., 2023, *AJ*, **165**, 42
- Ricci F., et al., 2015, *AJ*, **149**, 160
- Robertson B. E., Ellis R. S., Dunlop J. S., McLure R. J., Stark D. P., 2010, *Nature*, **468**, 49
- Rovero A. C., Donzelli C., Muriel H., Cillis A., Pichel A., 2013, in International Cosmic Ray Conference. p. 2676 ([arXiv:1307.6907](https://arxiv.org/abs/1307.6907)), doi:10.48550/arXiv.1307.6907
- Rovero A. C., Donzelli C., Pichel A., Muriel H., 2015, *arXiv e-prints*, p. [arXiv:1509.08377](https://arxiv.org/abs/1509.08377)
- Rovero A. C., Muriel H., Donzelli C., Pichel A., 2016, *A&A*, **589**, A92
- Sahu S., Páez-Sánchez D. I., Medina-Carrillo B., Pacheco-Aké R. d. J., Sánchez-Colón G., Rajpoot S., 2024, *MNRAS*, **533**, 2156
- Saldana-Lopez A., Domínguez A., Pérez-González P. G., Finke J., Ajello M., Primack J. R., Paliya V. S., Desai A., 2021, *MNRAS*, **507**, 5144

- Sandrinelli A., Treves A., Falomo R., Farina E. P., Foschini L., Landoni M., Sbarufatti B., 2013, *AJ*, 146, 163
- Shaw M. S., et al., 2012, *ApJ*, 748, 49
- Shaw M. S., et al., 2013, *ApJ*, 764, 135
- Taylor M. B., 2005, in Shopbell P., Britton M., Ebert R., eds, *Astronomical Society of the Pacific Conference Series Vol. 347, Astronomical Data Analysis Software and Systems XIV*. p. 29
- Torres-Zafra J., Cellone S. A., Buzzoni A., Andruchow I., Portilla J. G., 2018, *MNRAS*, 474, 3162
- Wakely S. P., Horan D., 2008, *International Cosmic Ray Conference*, 3, 1341
- de Menezes R., et al., 2019, *A&A*, 630, A55
- de Menezes R., et al., 2020, *Ap&SS*, 365, 12
- von Kienlin A., et al., 2020, *ApJ*, 893, 46

APPENDIX A: LONG TABLES: BEST CANDIDATES FOR OPTICAL OBSERVATIONS

This paper has been typeset from a $\text{\TeX}/\text{\LaTeX}$ file prepared by the author.

Table A1. This table lists the sources in the catalogue without redshift information, ordered by their $E_{\text{max}}^{\text{bin}}$. The first three columns show the source names, right ascension (R.A.), and declination (Dec.) in degrees (J2000), respectively. The fourth column presents redshift information obtained from the literature, with a ‘(?)’ flag for values that are uncertain or photometric, and a ‘>’ symbol for lower limits. The ‘z-origin’ column indicates the reference for the redshift information, using the short names described in Section 3.1. The column ‘b(deg)’ shows the galactic latitude in degrees, followed by the associated ‘4FGL-DR4’ name. Next, the column ‘ $TS_{10\text{GeV}}^{\text{ICGH}}$ ’ provides the Test Statistic value derived for ICGH sources detected above 10 GeV, integrating over 16 years of Fermi-LAT observations. The columns ‘ $E_{\text{max}}^{\text{bin}}$ ’ and ‘ τ_{Ebin} ’ list the highest energy bin detected and the corresponding EBL optical depth $\tau_{(E,z)}$, respectively. For sources whose Name’ begins with 4FGLJ, the R.A. and Dec. correspond to the associated counterpart position (see the ‘ASSOC1-4FGL’ column in, Ballet et al. 2023).

Name	R.A. (deg)	Dec. (deg)	z	z-origin	b(deg)	4FGLdr4	$TS_{E>10\text{GeV}}^{\text{ICGH}}$	$E_{\text{max}}^{\text{bin}}$	τ_{Ebin}
4FGLJ0537.8-6909	84.44756	-69.1721	-	-	-31.7	J0537.8-6909	267	714	-
4FGLJ1634.9+1222	248.76049	12.3619	-	-	35.8	J1634.9+1222	15	233	-
4FGLJ1933.9-1025	293.45639	-10.4242	-	-	-14.0	J1933.9-1025	15	185	-
3HSPJ013632.6+390559	24.13579	39.0997	-	-	-22.9	J0136.5+3906	4708	183	-
4FGLJ1705.5-7423	256.45043	-74.3777	-	-	-19.4	J1705.5-7423	40	169	-
4FGLJ1023.7+0038	155.94866	0.6448	-	-	45.7	J1023.7+0038	98	168	-
3HSPJ130738.0-425938	196.90825	-42.9941	-	-	19.7	J1307.6-4259	732	150	-
4FGLJ0840.1-0225	130.06121	-2.4531	-	-	22.7	J0840.1-0225	37	149	-
4FGLJ1334.1-3521	203.55010	-35.3372	-	-	26.7	J1334.1-3521	21	138	-
3HSPJ074642.0-475455	116.67629	-47.9152	-	-	-11.3	J0746.6-4754	1223	134	-
4FGLJ1544.9+3218	236.239	32.3035	-	-	52.2	J1544.9+3218	40	118	-
4FGLJ1305.4-4928	196.36448	-49.4681	-	-	13.3	J1305.4-4928	83	102	-
4FGLJ1554.2+2008	238.5533	20.1481	-	-	47.7	J1554.2+2008	71	100	-
3HSPJ230436.7+370507	346.15295	37.0854	-	-	-21.0	J2304.6+3704	297	98	-
3HSPJ102634.4-854314	156.64316	-85.7206	-	-	-23.6	J1027.0-8542	528	95	-
5BZBJ0700-6610	105.13017	-66.1792	-	-	-23.7	J0700.5-6610	986	94	-
3HSPJ230940.8-363248	347.42012	-36.5468	-	-	-66.5	J2309.7-3632	122	87	-
3HSPJ033349.0+291631	53.45416	29.2754	-	-	-21.5	J0333.7+2916	591	85	-
5BZBJ1849-4314	282.358	-43.2369	-	-	-17.8	J1849.4-4313	121	82	-
4FGLJ0703.2-3914	105.80268	-39.2385	-	-	-14.6	J0703.2-3914	52	81	-
4FGLJ1608.0-2038	241.98719	-20.6617	-	-	22.5	J1608.0-2038	50	80	-
4FGLJ2207.0+3607	331.78543	36.1597	-	-	-15.8	J2207.0+3607	49	79	-
3HSPJ130421.0-435310	196.0875	-43.8861	-	-	18.9	J1304.3-4353	1049	77	-
4FGLJ2345.9+3413	356.47985	34.2342	-	-	-26.7	J2345.9+3413	21	74	-
4FGLJ2143.9+3337	325.95889	33.6196	-	-	-14.7	J2143.9+3337	74	73	-
4FGLJ1345.6-3356	206.42935	-33.9453	-	-	27.5	J1345.6-3356	76	73	-
5BZBJ2108-6637	317.21592	-66.6229	-	-	-38.1	J2108.9-6638	198	73	-
4FGLJ0242.6-0000	40.66952	-0.0131	-	-	-51.9	J0242.6-0000	64	70	-
4FGLJ0836.0-8015	128.95466	-80.2696	-	-	-22.5	J0836.0-8015	29	69	-
4FGLJ2300.8-0736	345.22798	-7.5954	-	-	-57.3	J2300.8-0736	34	69	-
3HSPJ081012.0-703047	122.55016	-70.5130	-	-	-19.2	J0809.9-7028	12	68	-
4FGLJ1308.1-3801	197.04241	-38.0206	-	-	24.7	J1308.1-3801	19	67	-
3HSPJ104756.9-373730	161.98725	-37.6252	-	-	19.0	J1047.9-3738	45	65	-
4FGLJ1804.4+5249	271.09484	52.8205	-	-	28.2	J1804.4+5249	14	65	-
4FGLJ1438.5-4207	219.65309	-42.1185	-	-	16.4	J1438.5-4207	19	64	-
3HSPJ195547.9+021512	298.94941	2.2535	-	-	-13.2	J1955.7+0214	92	63	-
4FGLJ1836.5+1948	279.13380	19.8461	-	-	12.0	J1836.5+1948	54	62	-
5BZBJ0718-4319	109.68183	-43.3304	-	-	-13.6	J0718.6-4319	760	62	-
4FGLJ2118.2-5419	319.59207	-54.3406	-	-	-42.9	J2118.2-5419	26	62	-
4FGLJ2025.3-2231	306.31322	-22.5051	-	-	-30.1	J2025.3-2231	55	62	-
4FGLJ2127.6-5959	321.87039	-60.0137	-	-	-42.4	J2127.6-5959	16	60	-
4FGLJ0624.2-2943	96.09291	-29.7469	-	-	-18.4	J0624.2-2943	19	59	-
4FGLJ2049.0-4020	312.29171	-40.3419	-	-	-38.9	J2049.0-4020	19	59	-
3HSPJ151444.0-772254	228.68341	-77.3817	-	-	-16.6	J1514.4-7719	30	58	-

Table A2. This table lists the sources in the catalogue with uncertain redshift information, ordered by their $\tau_{(E,z)}$ values calculated at $E_{\text{max}}^{\text{bin}}$. The first columns show the source names, R.A., and Dec. in degrees (J2000), respectively. The fourth column presents redshift information from the literature, with a '(?)' flag indicating uncertain or photometric values and a '>' symbol denoting lower limits. The 'z-origin' column specifies the literature reference for the redshift, using the short names described in Section 3.1. The 'b(deg)' column shows the galactic latitude in degrees, followed by the associated '4FGL-DR4' name. The 'TS_{10GeV}^{ICGH}' column provides the Test Statistic value derived for ICGH sources detected above 10 GeV, integrating over 16 years of Fermi-LAT observations. The columns 'E_{max}^{bin}' and ' τ_{Ebin} ' list the largest energy bin detected and the corresponding EBL optical depth $\tau_{(E,z)}$, respectively. For sources whose Name' begins with 4FGLJ, the R.A. and Dec. correspond to the associated counterpart position(see the 'ASSOC1-4FGL' column in, Ballet et al. 2023).

Name	R.A. (deg)	Dec. (deg)	z	z-origin	b(deg)	4FGL-DR4	TS _{10GeV} ^{ICGH}	E _{max} ^{bin}	τ_{Ebin}
3HSPJ224753.2+441315	341.97175	44.22097	1.9(?)	Foschini22	-13.2	J2247.8+4413	375	179	5.08
3HSPJ015307.4+751742	28.28070	75.29522	2.35(?)	Foschini22	12.9	J0153.0+7517	168	149	4.94
4FGLJ0400.7+3920	60.18911	39.35271	1.1(?)	Foschini22	-10.2	J0400.7+3920	18	209	3.34
3HSPJ050756.2+673724	76.984	67.62341	0.34(?)	3HSPcat	15.8	J0507.9+6737	2936	406	1.73
3HSPJ200506.0+700439	301.27487	70.07763	2.32(?)	Foschini22	19.4	J2005.1+7003	311	66	1.60
5BZBJ0428-3756	67.16842	-37.93878	>1.02	Landoni15	-43.6	J0428.6-3756	5673	119	1.24
3HSPJ052542.4-601340	81.42675	-60.22783	1.78(?)	Kaur16	-33.8	J0525.6-6013	249	70	1.21
4FGLJ1937.0+8354	294.41522	83.94139	1.94(?)	Foschini22	25.7	J1937.0+8354	39	61	1.12
4FGLJ1858.1+7318	284.58486	73.28700	0.471(?)	Foschini22	25.4	J1858.1+7318	43	221	1.10
3HSPJ031612.7+090443	49.05304	9.07866	0.372(?)	3HSPcat	-39.5	J0316.2+0905	621	255	0.99
3HSPJ142829.9+743002	217.12454	74.50061	0.31(?)	3HSPcat	41.0	J1428.8+7429	18	294	0.95
3HSPJ144800.6+360831	222.00245	36.142	>0.738	Paiano20	63.7	J1448.0+3608	1085	137	0.94
5BZBJ1248+5820	192.07825	58.34131	0.508(?)	Foschini22	58.7	J1248.3+5820	4149	189	0.94
5BZBJ0007+4712	1.99988	47.20214	>1.659	Shaw13	-15.0	J0008.0+4711	709	61	0.87
3HSPJ122337.0-303250	185.90420	-30.54725	>0.875	Desai19	31.9	J1223.6-3032	76	113	0.87
4FGLJ0318.7+2135	49.69028	21.57685	1.83(?)	Foschini22	-29.6	J0318.7+2135	171	55	0.85
3HSPJ063059.5-240646	97.748	-24.11280	>1.239	3HSPcat	-14.9	J0630.9-2406	3589	78	0.80
5BZBJ1918-4111	289.56687	-41.19189	>1.591	Shaw13	-22.2	J1918.2-4111	555	60	0.79
5BZBJ1925-2219	291.41579	-22.32642	1.35(?)	Foschini22	-17.1	J1925.8-2220	37	69	0.76
5BZBJ2300+3137	345.09512	31.61789	>1.498	Shaw13	-25.5	J2300.3+3136	283	62	0.76
5BZBJ1314+2348	198.68254	23.80744	2.053(?)	SDSSdr18	83.7	J1314.7+2348	387	46	0.76
4FGLJ0453.1+6322	73.30189	63.35496	2.1(?)	Foschini22	12.1	J0453.1+6322	39	45	0.75
3HSPJ154015.1+815505	235.06625	81.91822	>0.67	Paiano17	32.9	J1540.1+8155	938	129	0.72
3C 66A	35.67334	43.04319	>0.3347	Furniss13	-16.7	J0222.6+4302	7060	230	0.70
5BZBJ0856-1105	134.17421	-11.08733	>1.397	Shaw13	21.4	J0856.6-1105	517	64	0.70
5BZBJ0612+4122	93.21325	41.37706	>1.107	Paiano20	10.9	J0612.8+4122	1383	80	0.68
3HSPJ181118.0+034113	272.82508	3.68711	0.717(?)	Foschini22	10.6	J1811.3+0340	473	117	0.67
3HSPJ043145.1+740326	67.93775	74.05738	1.35(?)	Foschini22	17.3	J0431.8+7403	226	65	0.67
3HSPJ103744.3+571155	159.43458	57.19880	>0.62	Meisner10	51.7	J1037.7+5711	3071	131	0.65
3HSPJ003514.1+151504	8.81129	15.25116	>0.64	3HSPcat	-47.4	J0035.2+1514	485	122	0.60
3HSPJ112048.1+421212	170.20025	42.2035	>0.35	3HSPcat	66.1	J1120.8+4212	1811	199	0.58
S5 0716+714	110.47250	71.34332	0.31(?)	Foschini22	28.0	J0721.9+7120	11282	218	0.57
3HSPJ170433.8-052840	256.14095	-5.47797	>0.7	Paiano17	20.7	J1704.5-0527	244	109	0.55
3HSPJ152048.9-034851	230.20370	-3.81433	>0.868	Goldini20	42.5	J1520.8-0348	421	88	0.53
3HSPJ193419.6+600139	293.58175	60.02763	1.38(?)	Foschini22	18.1	J1934.2+6002	44	56	0.52
4FGLJ1304.2-2412	196.06955	-24.20465	1.26(?)	Foschini22	38.5	J1304.2-2412	155	60	0.51
5BZBJ1312-2156	198.1315	-21.93983	>1.485	Shaw13	40.6	J1312.4-2156	358	50	0.50
4FGLJ0028.5+2001	7.12424	20.00742	1.552(?)	4LACdr3	-42.5	J0028.5+2001	489	48	0.50
3HSPJ175615.1+552218	269.06625	55.37166	>0.657	3HSPcat	29.7	J1756.3+5522	264	106	0.47
4FGLJ0355.3+3909	58.81912	39.15272	0.846(?)	Foschini22	-11.0	J0355.3+3909	18	85	0.47
3HSPJ210421.9-021238	316.09137	-2.21080	>0.45	3HSPcat	-30.3	J2104.3-0212	88	140	0.43
3HSPJ222129.3-522527	335.37208	-52.4243	>0.34	3HSPcat	-52.3	J2221.5-5225	426	174	0.42
3HSPJ125359.3+624257	193.49725	62.716	>0.867	Shaw13	54.4	J1253.8+6242	179	79	0.42
4FGLJ1537.9-1344	234.48793	-13.7262	0.984(?)	Foschini22	32.5	J1537.9-1344	31	70	0.42